Ecological Engineering 113 (2018) 43–51

Contents lists available at ScienceDirect

Ecological Engineering

journal homepage: www.elsevier.com/locate/ecoleng

Effectiveness of a bubble-plume mixing system for managing phytoplankton in lakes and reservoirs

Shengyang Chen[a], Cayelan C. Carey[b], John C. Little[c], Mary E. Lofton[b], Ryan P. McClure[b], Chengwang Lei[a,*]

[a] School of Civil Engineering, The University of Sydney, Sydney, NSW 2006, Australia
[b] Department of Biological Sciences, Virginia Tech, Blacksburg, VA 24061, USA
[c] Department of Civil and Environmental Engineering, Virginia Tech, Blacksburg, VA 24061, USA

ARTICLE INFO

Keywords:
Bubble-plume mixing
Hydrodynamics
Ecological modelling
Biogeochemical modelling
Phytoplankton management
Algal blooms

ABSTRACT

Bubble-plume mixing systems are often deployed in eutrophic lakes and reservoirs to manage phytoplankton taxa. Unfortunately, inconsistent outcomes from bubble-plume (induced) mixing are often reported in the literature. The present study investigates the response of phytoplankton to induced mixing using a whole-reservoir field experiment and a three-dimensional hydrodynamic model (Si3D) coupled with the Aquatic EcoDynamics (AED) model through the framework for aquatic biogeochemical modelling (FABM). The coupled Si3D-AED model is validated against a 24-h field mixing experiment and subsequently used for a numerical parametric study to investigate phytoplankton responses to various induced mixing scenarios in which the phytoplankton settling rate, phytoplankton growth rate, reservoir depth, and mixing system diffuser depth were sequentially varied. Field observations during the mixing experiment suggest that the total phytoplankton concentration (measured in μg/L) across the reservoir was reduced by nearly 10% during the 24-h mixing period. The numerical modeling results show that phytoplankton concentration may be substantially affected by the functional traits of the phytoplankton and the deployment depth of the mixing diffuser. Interestingly, the numerical results indicate that the phytoplankton concentration is controlled by reduced growth rates due to light limitation in deep reservoirs (> 20 m), whereas settling loss is a more important factor in shallow reservoirs during the mixing period. In addition, the coupled Si3D-AED model results suggest that deploying the mixing diffuser deeper in the water column to increase mixing depth may generally improve the successful management of cyanobacteria using bubble-plume mixing systems. Thus, the coupled Si3D-AED model introduced in the present study can assist with the design and operation of bubble-plume mixing systems.

1. Introduction

Bubble-plume mixing systems, a type of water quality management system, are increasingly deployed to manage phytoplankton in lakes and reservoirs (Imteaz and Asaeda, 2000; Heo and Kim, 2004; Visser et al., 2016). Many studies have reported that turbulent mixing induced by mixing systems may mitigate water quality problems, including algal blooms and hypolimnetic hypoxia (e.g., Huisman et al., 2004; Imteaz et al., 2009; Gerling et al., 2014; Lehman, 2014).

Despite their increasing use by water managers, there has been little guidance as to how to best deploy and operate mixing systems for phytoplankton management. As a consequence, many mixing systems have been unable to prevent phytoplankton blooms, which are increasing globally due to climate and land use change, and can result in scums, odors, and toxins in drinking water supplies (Brookes and Carey, 2011; Carey et al., 2012). A study conducted by Nürnberg et al. (2003) showed that improper continuous mixing and aeration throughout a year may increase surface phytoplankton blooms due to increased upwelling of nutrients. Furthermore, poor design and operation of a mixing system may destratify a water body before fall turnover, impairing water quality. Toffolon et al. (2013) reported that mixing which aimed to increase dissolved oxygen (DO) in a shallow reservoir caused undesired premature destratification and even reduced the hypolimnetic DO concentration. Thus, careful consideration of the intensity, duration, and frequency of mixing is required for successful deployment of this type of water-quality management systems.

Additionally, the appropriate depth of deployment for mixing systems may vary based on taxon-specific phytoplankton traits and water body depth. Different phytoplankton taxa (e.g., cyanobacteria, green

* Corresponding author.
E-mail address: chengwang.lei@sydney.edu.au (C. Lei).

https://doi.org/10.1016/j.ecoleng.2018.01.002
Received 21 September 2017; Received in revised form 3 December 2017; Accepted 2 January 2018
Available online 08 February 2018
0925-8574/

algae, or diatoms) respond differently to vertical mixing (Huisman et al., 2004; Lehman, 2014). Generally reservoir managers try to promote the growth of diatoms and limit the growth of cyanobacteria (Bielczyńska, 2015; Visser et al., 2016) because cyanobacteria are primarily responsible for harmful blooms in fresh water bodies (Carey et al., 2012). Their positive buoyancy due to gas vesicles allows cyanobacteria to dominate in the surface waters, maximizing incoming light for their growth (Visser et al., 1997; Huisman et al., 2004). Many studies have reported that the growth rate of bloom-forming cyanobacteria decreases due to the light limitation that occurs when turbulent mixing induced by mixing systems entrains cyanobacteria into deeper water (e.g., Nürnberg et al., 2003; Huisman et al., 2004). Field and numerical modelling studies suggest that vertical mixing prevents the growth of cyanobacteria but favours diatoms, which would otherwise quickly sink out of the photic zone in the absence of mixing due to their dense silica frustules (Huisman et al., 2005). As a result, induced mixing may result in a shift of the dominant taxa from bloom-forming cyanobacteria to diatoms. Therefore, particularly in deep water bodies with large aphotic zones, mixing may affect phytoplankton concentration by changing the competition for light among different species (Reynolds, 2006).

In shallow water bodies, however, the aphotic zone is much thinner (e.g., Nürnberg et al., 2003). Phytoplankton cells may settle out quickly on the sediments of shallow water bodies, setting up a scenario where settling rates, rather than light-dependent growth rates of different phytoplankton groups, may determine the overall outcome of mixing (Condie, 1999). Thus, the depth of a lake or reservoir may be an important factor controlling the outcome of mixing in water bodies. An optimum mixing depth controlled by the diffuser depth and mixing intensity may exist for a given water body, achieving a balance between managing phytoplankton taxa while simultaneously preserving thermal stratification.

To determine how best to deploy and operate water-quality management systems, we operated a bubble-plume mixing system in a shallow drinking water supply reservoir to examine its effects on phytoplankton. We used the experimental results to calibrate a 3-D hydrodynamic model (described in Chen et al., 2017) and then modelled multiple scenarios in which we sequentially manipulated the settling rate, phytoplankton growth rate, reservoir depth, and diffuser depth for idealized phytoplankton (cyanobacteria and diatom) cells. Our goal was to understand the effects of bubble-plume mixing on phytoplankton dynamics and improve the management outcomes following deployment of bubble-plume mixing systems in lakes and reservoirs.

2. Methodology

2.1. Study site

The study site is eutrophic Falling Creek Reservoir (FCR) in Vinton, Virginia, USA (37°18′12″N, 79°50′14″W). FCR is managed by the Western Virginia Water Authority (WVWA) for drinking water supply. The bathymetry of FCR is shown in Fig. 1. The reservoir has two water-quality management systems (a side-stream supersaturated hypolimnetic oxygenation system, SSS, and a bubble-plume epilimnetic mixer, EM) installed to deal with summer hypoxia and phytoplankton blooms, respectively.

The SSS system is designed to increase DO in the hypolimnion and suppress the release of soluble iron, manganese and phosphorus from the sediments, without destratifying the reservoir. The purpose of the EM system is to simultaneously mix and deepen the mixed layer, thereby disrupting the growth of surface bloom-forming phytoplankton taxa (e.g., cyanobacteria) by decreasing their access to light. Detailed descriptions of the SSS and EM systems are provided in previous studies (Gerling et al., 2014; Chen et al., 2017).

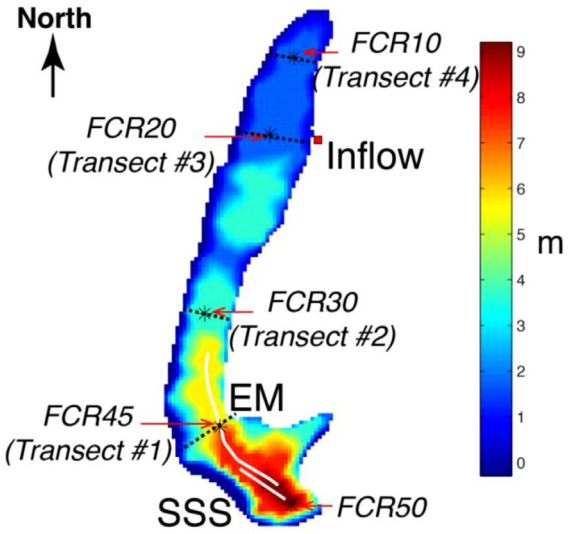

Fig. 1. FCR bathymetry and sampling locations. White lines near the deepest site of the reservoir, FCR50, show the locations of the SSS and EM systems. Black dashed lines in the contour show the location of Transects #1–#4.

2.2. Field experiment

Mixing experiments were carried out during summer 2016 to investigate the effect of bubble-plume mixing on phytoplankton dynamics across the water body. The schedule of operation for the EM system is shown in Table 1. The EM system was operated continuously over a 24-h period, whereas the SSS system remained in operation throughout the study.

There were five monitoring locations (FCR10, FCR20, FCR30, FCR45, and FCR50) in the thalweg from the upstream of the reservoir to the downstream (Fig. 1). The four upstream locations had corresponding transects (#1–#4), each consisting of nine monitoring points evenly distributed laterally across the reservoir, as indicated by the black dashed lines in Fig. 1. In total, there were 37 monitoring locations where vertical profiles were collected during the experimental period.

Temperature, dissolved oxygen (DO), and chlorophyll-a profiles were collected with an SBE 19plus high-resolution (4 Hz sampling rate) Conductivity, Temperature, and Depth (CTD) profiler (Sea-Bird Scientific, Bellevue, WA, USA) attached with a WETLabs ECO-FL fluorometer (Sea-Bird Scientific, Bellevue, WA, USA). The vertical resolution measured by the CTD was at ~ 0.1m for each of the 37 monitoring profiles from the water surface to the bottom. One-minute resolution meteorological data were obtained from an *in-situ* weather station deployed on the dam of FCR (Campbell Scientific Inc., UT, USA). The quality of the data collected by the weather station was checked against meteorological data measured at Roanoke Airport, which were downloaded from the National Climatic Data Center of the National Oceanic and Atmospheric Administration (NOAA, www.ncdc.noaa.gov).

Table 1
Experimental schedule for the EM system.

DoY	178	179	180
EM	OFF	ON	OFF

2.3. Numerical simulation

2.3.1. Si3D hydrodynamic model

The Si3D hydrodynamic model, a semi-implicit 3-D computational fluid dynamics code, was adopted in this study. The locations of the SSS and EM systems in the model were the same as their corresponding locations in the field as shown in Fig. 1. The model employed a finite-difference method for numerical solution of the Navier-Stokes equations (Rueda and Schladow, 2003; Rueda et al., 2007). Three sets of governing equations were solved by the model, including the continuity equation, momentum equations, and the scalar transport equations (Smith, 2006).

A bubble-plume model (Wüest et al., 1992) was employed to simulate the flow induced by the EM system, which releases air bubbles from a linear diffuser into water. Application and validation of the linear bubble-plume model were described by Singleton et al. (2007, 2009). The bubble-plume model estimated the depth of the maximum plume rise (DMPR) dynamically under the condition that the momentum of the rising plume is zero at the DMPR. The mixing induced by the SSS system was simulated by a coupled water-jet model in Si3D (Chen et al., 2017). Full validation of the two coupled models embedded within Si3D has been described by Chen et al. (2017).

2.3.2. Coupled AED model

Si3D was developed to conform to the protocol of the Framework for Aquatic Biogeochemical Modelling (FABM, Bruggeman and Bolding, 2014), coupling with the Aquatic EcoDynamics (AED) model (Hipsey et al., 2013). A coupling scheme between Si3D and the AED model is shown in Fig. 2. In the coupled AED model of Si3D, all of the modules in the AED model can interactively simulate a range of the state variables simultaneously, including DO concentration, sediment fluxes, carbon, silica, nitrogen, phosphorus, organic matter, phytoplankton, and zooplankton. The coupled AED model in the present study adopted the modules for DO concentration and phytoplankton with relevant phytoplankton parameters shown in Appendix 1.

With the 3-D hydrodynamic model Si3D hosting the simulation, the AED model was able to predict phytoplankton dynamics in three dimensions. The DO module in the AED model was enabled to simulate oxygen exchanges from the bubble-plume mixing system and the SSS system. All of the model inputs other than the AED parameters (e.g., time steps, grid resolution) and physical data (e.g., air/water temperatures) required by the AED model were synchronized with Si3D.

2.3.3. Resuspension of phytoplankton cells

Water flowing close to the sediments may re-suspend phytoplankton cells that settle on the sediments. According to James et al. (2004), the critical shear stress τ_c for fine-grained sediment resuspension is 0.14 Pa (1.4 Dynes/cm^2), below which the resuspension is negligible. The sizes of phytoplankton cells are in the range of 1–100 μm (Durham et al., 2013), which is close to the size of fine-grained sediment. Since the average density of phytoplankton cells is above 1050 kg/m^3, with the density of diatoms generally over 1100 kg/m^3 (Reynolds, 2006), their density difference with water (~ 100kg/m^3) is close to the mean density difference between water and sediments for a similar range of particle sizes reported in the literature (e.g., Khelifa and Hill, 2006; Curran et al., 2007; Chiou et al., 2012). Therefore, the fine-grained sediment resuspension shear stress is adopted as the critical shear stress to determine possible re-entrainment of phytoplankton cells from the sediments by flowing water. The potential maximum shear stress was estimated in the following two ways:

First, a lake-wide suspended sediment model developed by Bailey and Hamilton (1997) was used to calculate the shear stress on the sediments in water. The model accounted for the effect of wave action induced by winds over the water surface to estimate the shear stress at the sediment-water interface. The theoretical bottom stress τ was calculated as:

$$\tau = H\left[\frac{\rho(\nu(2\pi/T)^3)^{0.5}}{2\sinh(2kh)}\right] \quad (1)$$

In Eq. (1), H is the wave height (m), ρ is the density of water (kg/m^3), T is the wave period (s), ν is the kinematic viscosity (m^2/s), k is the wave number ($2\pi/L$ where L = wavelength,m), and h is the water depth (m). H, T, and L can be obtained, based on the maximum wind speed and water depth, from the a model reported in Coastal Engineering Research Center (1984). The estimated maximum shear stress τ_{max} in FCR is 2.23×10^{-2}Pa (0.23Dynes/cm^2) using a shallow depth near the sidearm (~ 1m). Since τ_{max} is nearly one order of magnitude smaller than the critical shear τ_c, the bottom shear stress tends to be insignificant for sediment resuspension in FCR.

Second, the velocity gradient obtained from the coupled Si3D model close to the sediments was used to calculate the shear stress induced by

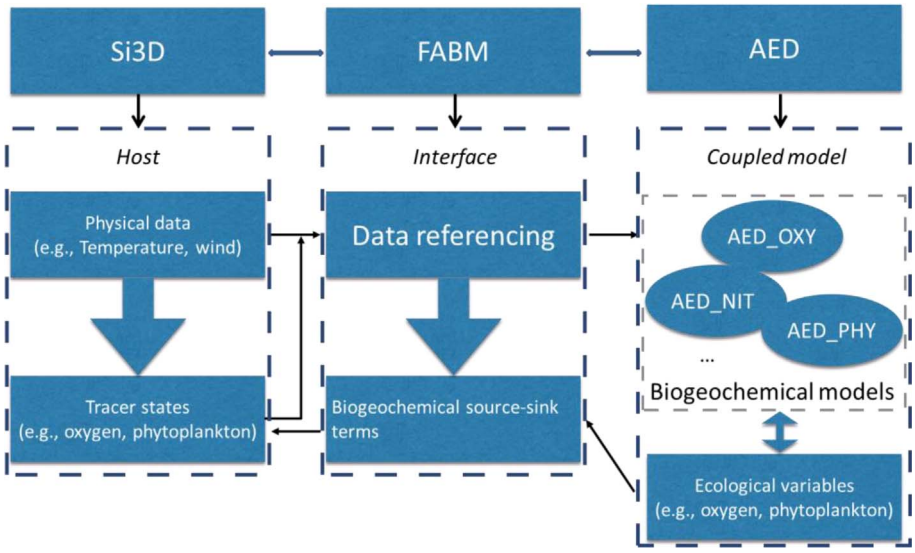

Fig. 2. Coupling process for Si3D-FABM-AED.

Table 2
Simulation cases of various settling rates and growth rates.

Cases	Maximum Depth (m)	Settling Rate (m/d)	Growth Rate (d^{-1})	Diffuser Depth (m)
0 (reference)	9.3	1.2	0.12	5.00
1	9.3	0.5	0.00	5.00
2	9.3	1.2	0.00	5.00
3	9.3	2.4	0.00	5.00
4	9.3	5.0	0.00	5.00
5	9.3	1.2	0.06	5.00
6	9.3	0.5	0.12	5.00

flows near the sediments. If the boundary condition of the sediments is a no-slip condition, the maximum shear stress can be calculated as:

$$\tau = \mu\frac{du}{dz} = \mu\frac{u_b - 0}{z_b} \quad (2)$$

where μ is the dynamic viscosity of water Pa·s, u_b is the model-estimated average velocity (m/s) of the numerical cell adjacent to the sediments during the mixing period with intense flows, and z_b is the half height of the numerical cell adjacent to the sediments. From the calculation, it is found that $\tau_{max} = 5.23 \times 10^{-4}$ Pa (5.23×10^{-3} Dynes/cm^2), which is also much smaller than τ_c. Therefore, possible phytoplankton cell resuspension is again deemed negligible after cell settling on the sediments based on the above estimated maximum shear stresses.

2.3.4. Horizontal mobility of phytoplankton cells

The horizontal mobility of most phytoplankton ranges from under 0.1 mm/s to about 0.5 mm/s (Eppley et al., 1967; Kamykowski and McCollum, 1986). Compared to the typical flow velocities in the hypolimnion obtained in the model (~3.0 mm/s), the horizontal mobility is an order of magnitude slower. In a relatively short period of induced mixing at high velocity, the horizontal mobility of phytoplankton cells is negligible compared to the mixing-induced flows in water, and thus is not considered here.

2.4. Model validation

The thermal structure obtained from the coupled Si3D model has been validated in a previous study (Chen et al., 2017); therefore, this study focused on comparing the predicted phytoplankton results with the field chlorophyll-a data collected using the CTD during the mixing experiment. The comparison was based on the reference case shown in Table 2 and Appendix 1.

After the model was spun up for up to a week and before the numerical mixing experiment took place, an initialization for phytoplankton concentrations was carried out with customized modules in Si3D. Spatial profiles of phytoplankton concentrations in the model were obtained from the field chlorophyll-a data recorded by the CTD at the four transects (refer to Fig. 1) immediately before the mixing experiment. The nearest-neighbor interpolation method (Parker et al., 1983) was adopted to fill in data gaps in the model.

From the validation, both the distribution of the modeled phytoplankton concentration and time series of the phytoplankton concentration in water are in reasonable agreement with the field data, as shown in Figs. 3 and 4a-b. The trend of the phytoplankton movement is correctly predicted by the coupled hydrodynamic model. The difference in the phytoplankton concentration vertically in the littoral region (FCR10-30) is estimated by differentiating the layer-averaged concentration before and during the mixing experiment, as shown in Fig. 4c, which also compares the difference in concentration between the field and numerical results. Both numerical results and field data consistently suggest an increase of the phytoplankton concentration near the 3 m depth in the littoral region under induced mixing. The difference of the average chlorophyll-a concentration of the simulation compared to the field data is less than 3.6% during the mixing experiment. Therefore, the coupled hydrodynamics model may be adopted to model the phytoplankton dynamics with confidence.

3. Results and discussion

The present numerical parametric study investigated phytoplankton dynamics in the water body during induced mixing using the coupled Si3D-AED model. To improve the design and operation of bubble-plume mixing systems for phytoplankton management, the dependence of management outcomes from induced mixing on the settling rate of phytoplankton, the growth rate of phytoplankton, the reservoir depth, and the diffuser depth of the bubble-plume mixing system was quantified.

First, the settling and growth rate of phytoplankton were changed, with the rest of the parameters fixed to investigate phytoplankton responses to induced mixing (Section 3.1). Next, the maximum depth of the water body was altered in Section 3.2 to examine the effects of the reservoir depth on phytoplankton responses to induced mixing. Finally, the effects of varying the diffuser depth, which resulted in the change of mixing depth and intensity, were investigated in Section 3.3. For comparison among the various scenarios, the results presented in the following sections will use the difference in the phytoplankton concentrations calculated by subtracting the predicted concentration in the case with bubble-plume mixing from that in the corresponding case without bubble-plume mixing.

3.1. Effects of phytoplankton traits

The cases for studying the effects of phytoplankton traits in the simulation are shown in Table 2. We focused on functional trait groups of phytoplankton for this modelling study to follow the precedent of many earlier phytoplankton modelling studies (reviewed by Rigosi et al. (2010)), and because species-level data were not available. Case 0 is a reference case with an average settling rate of phytoplankton (Reynolds et al., 1987) and a realistic growth rate of phytoplankton in natural water bodies (Welschmeyer and Lorenzen, 1985). The growth rates and settling effects are discussed with Case 0, followed by a series of case studies (Cases 1–6) based on the two factors. Cases 1–4 represent idealized phytoplankton cells with different settling rates, i.e., cyanobacteria ($< \sim 1.0$ m/d) and diatoms ($> \sim 2.0$ m/d) (Reynolds et al., 1987). The growth rates of phytoplankton in the model for Cases 5 and 6 were within the range observed by Welschmeyer and Lorenzen (1985).

3.1.1. Reference case

The reference case (Case 0) shows substantial reduction of the phytoplankton concentration over a relatively short time, as observed in Fig. 4b. The significant reduction of the cells associated with the induced mixing is likely attributed to the effect of cell settling in the shallow water body. This suggests that, when the bubble-plume mixing is in operation, the growth rate of phytoplankton is much lower than the settling rate of phytoplankton in shallow water bodies.

Because of the dominance of the settling effect, the phytoplankton settling loss is examined first using the idealized species with a range of settling rates (Cases 1–4) with growth rates set to zero, as described below. Subsequently, the influence of growth rate on the phytoplankton dynamics under induced mixing is investigated in Cases 5–6.

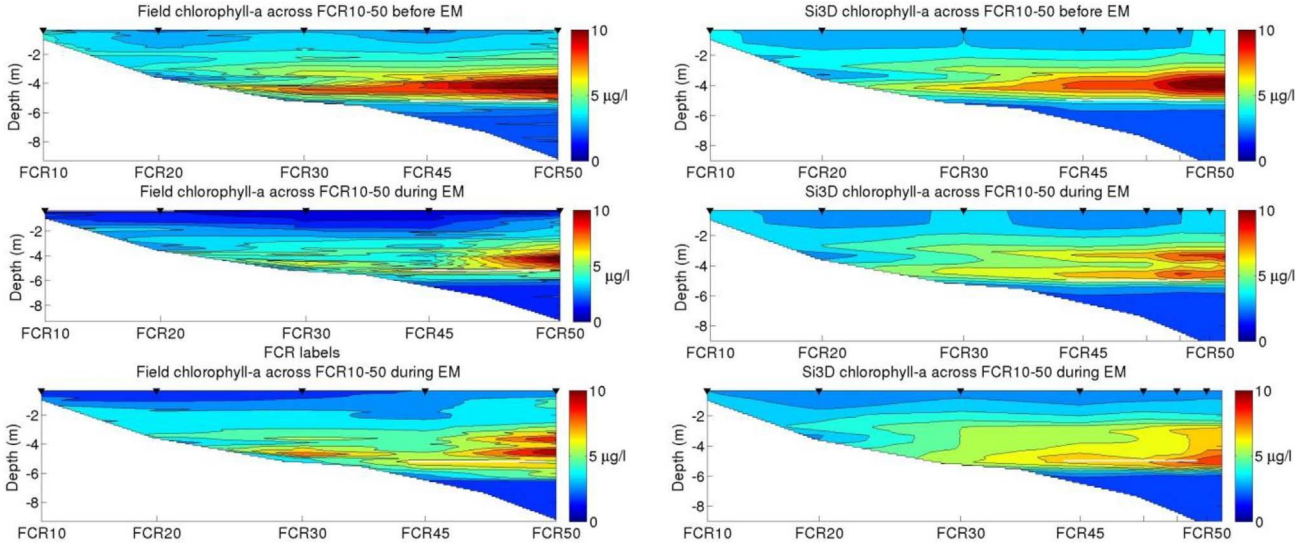

Fig. 3. Field phytoplankton concentration distribution (left) vs. numerical phytoplankton tracer concentration (right) obtained from the coupled Si3D model. Time instant from top to bottom: 0 h, 3 h, and 6 h during the experiment. Dark inverse triangles on the top indicate the sampling points in the field and model, respectively.

3.1.2. Settling effect

In Case 2, which has the same settling rate as Case 0, the mean horizontal fluxes of the normalized phytoplankton concentration ($m^{-2}s^{-1}$, normalized by the initial phytoplankton concentration) at Transect #2 go dominantly towards the littoral region during the mixing period, as shown in Fig. 5a when the bubble-plume mixing system is in operation. The time-moving-averaged fluxes (in red), with a window size of half an hour, demonstrate a distinct shift of the phytoplankton fluxes during and after the mixing period. The observation suggests that the majority of phytoplankton cells are carried from the deep region to the littoral region by the mixing-induced flows.

The net movement of phytoplankton cells from the deep region to the littoral region during induced mixing increases the likelihood of their settling onto the sediments. This is because sinking cells will reach the sediments faster at a site in the littoral region (vs. the deep region). Further evidence demonstrating the trend for the cell settling loss is shown in Fig. 5b overlaid by the dashed line for Transect #2, which separates the littoral and deep regions. Due to more intensive fluxes towards the littoral region at Transect #2 during mixing (at 6 h in Fig. 5a), more phytoplankton cells are transported to the littoral region and settle out from the water quickly, which is confirmed by an increase of the phytoplankton concentration immediately above the sediments during induced mixing (Fig. 5b). As a result, the transport of cells upstream to the littoral region is found to be a very important mechanism in shallow water bodies (e.g., FCR) for reducing phytoplankton during induced mixing.

To specifically investigate the settling effect, the cases with a range of settling rates are simulated using the coupled Si3D-AED model (Case 1–4). Each curve in Fig. 6 shows the difference in the concentration of phytoplankton obtained from the simulations with and without bubble-plume mixing imposed. In the plots, a negative value means that the mixing reduces the overall phytoplankton concentration across the reservoir, in comparison to the simulation without induced mixing imposed.

Based on the phytoplankton behaviour identified above (Fig. 6a), the induced mixing in the deep region of the water body facilitates the settling loss of cells with a lower sinking rate (e.g., cyanobacteria as typically indicated in Case 1). The detrained flows induced by bubble-plume mixing carry the phytoplankton cells from the deep region towards the shallow region. However, this is not the case for cells with greater sinking rates (i.e., diatoms, as indicated in Case 3). The induced mixing hinders the settling of heavier cells, resulting in an increase of phytoplankton concentrations compared to the scenario without induced mixing (Case 4 in Fig. 6a). Therefore, induced turbulent mixing in shallow reservoirs may change the competition among phytoplankton taxa, the outcome of which is consistent with findings from mixing in deep water bodies (Huisman et al., 2004; Visser et al., 2016), even though the mechanism leading to the mixing outcome is different (light limitation vs. settling effect).

3.1.3. Growth effect

To investigate the effect of growth rate of phytoplankton on the aforementioned outcome of bubble-plume mixing, a dimensionless growth parameter G is used to characterize the relative importance of growth and settling (Condie and Bormans, 1997; Condie, 1999), that is,

$$G = R_G h / v_s$$

where R_G is the growth rate (d^{-1}) of the species; h is the maximum depth of the water body (~ 9.3m); and v_s represents the sinking rate (m/d). The cases with different growth parameters for comparison and with all the other parameters kept unchanged (refer to Table 2) are shown in Table 3.

By definition (Condie, 1999), the settling effect dominates the concentration of phytoplankton when $G < 1$. For $G > 1$, the growth more than compensates the settling loss. Accordingly, as shown in Fig. 6b, when the growth rate becomes a dominant effect in controlling cell concentration, i.e., $G > 1$ (Case 6), induced mixing enhances the cell settling, resulting in greater reduction in phytoplankton concentration compared to the case with a lower G (Cases 0, 2, 5). The results suggest that induced mixing could be more effective for reducing phytoplankton in the case with a higher G when the growth rate outweighs the settling loss (Fig. 6b).

3.2. Effects of bathymetry

A numerical study for water bodies with different water depths is carried out in idealized reservoirs with modified bathymetry based on FCR, in which depths of water in all places of the reservoir are set to be proportional to the maximum water depth. To maintain the same energy input per unit volume of water during bubble-plume mixing, the diffuser depth of the EM system is adjusted according to the maximum water depth for each case with the modified bathymetry (see Table 4). The flow rate of the EM system is also calibrated to ensure that the DMPRs in all the cases are the same within the mixed layer, where the phytoplankton cells often accumulate. Two important factors that may control the cell concentration in water are examined: the light

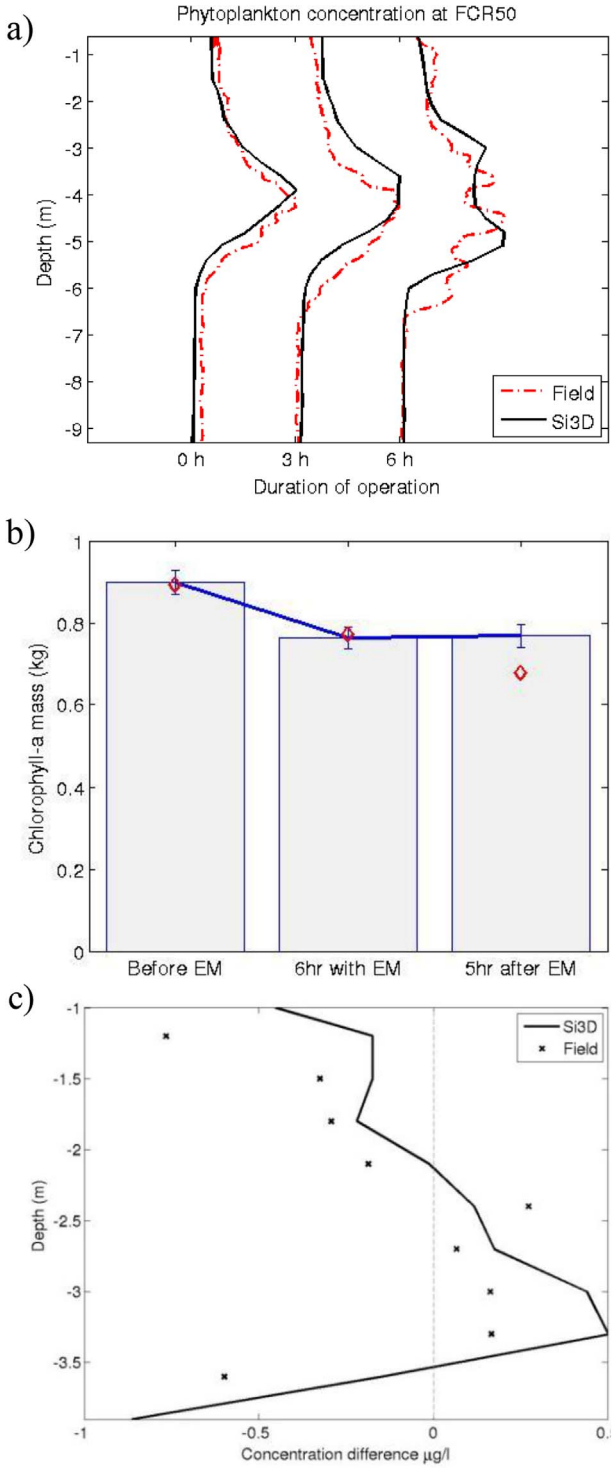

Fig. 4. a) Phytoplankton concentration profiles at FCR50; b) total reservoir-integrated chlorophyll-a mass during EM mixing: comparison between field data (red line) and Si3D results (red diamond). c) Difference of layer-averaged phytoplankton concentration before (0 h) and during mixing (at 6 h) between FCR10 and FCR30: field data vs Si3D results. (For interpretation of the references to colour in this figure legend, the reader is referred to the web version of this article.)

limitation of phytoplankton growth and their settling loss.

The results shown in Fig. 7 compare the normalized reduction in the phytoplankton concentration due to the effect of light limitation and settling loss in water bodies of different depths. The data indicate that the relative importance of the two factors could switch, depending on the maximum depth of the water body under induced mixing. In relatively shallow water bodies (i.e., maximum depth $< \sim 20$ m), light limitation has less impact on the phytoplankton concentration than settling loss, because photosynthetically active radiation (PAR) is more likely to penetrate through the water column to reach the hypolimnion. As a result, the aphotic zone in shallow water bodies is much smaller than in deep water bodies. Shallow water bodies are more likely to have sufficient PAR to meet the critical light intensity for the growth of phytoplankton cells even close to the sediments. Therefore, light intensity may not be a limiting factor for phytoplankton cells in this scenario, even though induced mixing may push the cells into deep water. Consequently, settling loss of phytoplankton cells in shallow water bodies is found to be a more important factor driving phytoplankton concentration than light limitation, as noted above. The phytoplankton dynamics identified here also explain why the growth effect was not as important as the settling effect discussed above in Section 3.1 for the reference case.

For deeper reservoirs (i.e., maximum depth $> \sim 20$ m), the results suggest that light limitation plays a more important role in phytoplankton responses to mixing than settling loss (Fig. 7). Since deeper water bodies have a larger aphotic zone, less PAR can reach the hypolimnion, reducing light availability for phytoplankton growth. If the cells are moved into the aphotic zone by induced mixing, the growth rate of phytoplankton is constrained due to light limitation.

In contrast, settling loss in deeper water bodies is reduced because it takes longer for cells to settle to the sediments. Thus, in deeper water bodies, phytoplankton growth rate may compensate the effect of settling loss due to the extended settling time, resulting in minimal influence of the settling loss on phytoplankton concentrations.

3.3. Effect of diffuser depth

The effect of diffuser depth on phytoplankton concentrations is examined using the case with a maximum depth of 28 m. With a deeper diffuser depth as shown in Table 5 but the same DMPR, both the mixing depth and mixing intensity are increased. Corresponding results of mixing are shown in Fig. 8. For comparison, the results from the reference case are also shown in the figure.

The outcome of bubble-plume mixing for managing phytoplankton concentrations is improved if the diffuser is deployed at a deeper depth (see Cases 11, 13, 14 in Fig. 8). Interestingly, when the diffuser is placed near the surface, as for Case 0 and Case 13, the shallow and deep water bodies exhibit a similar reduction rate of phytoplankton concentration during induced mixing, with a difference of less than $\sim 0.6\%$ of the initial concentration by the end of the mixing period. This finding reveals the importance of the design and operation of the mixing system for managing phytoplankton in a water body, as optimal outcomes in terms of phytoplankton management may not be achieved without proper system design. In deeper water bodies, the mixing outcome can be improved by placing the diffuser deeper in the water while keeping the DMPR the same, as confirmed by the better outcome from Case 14 than the others (maximum difference of the phytoplankton is over 5.2% within the mixing period). These data suggest that increasing mixing depth and mixing intensity could enhance the transport of the phytoplankton cells into deeper water. Accordingly, the extent to which the phytoplankton concentration is reduced by induced mixing may depend on the mixing depth and the mixing intensity, in addition to the traits of the phytoplankton taxa.

3.4. Summary

The results show that induced mixing has strong effects on phytoplankton dynamics in reservoirs. In shallow water bodies, the settling effect of phytoplankton cells is an important mechanism driving the reduction of phytoplankton during mixing. Induced mixing may enhance the settling loss of some bloom-forming taxa (e.g., cyanobacteria) in shallow regions of the water body, while increasing the

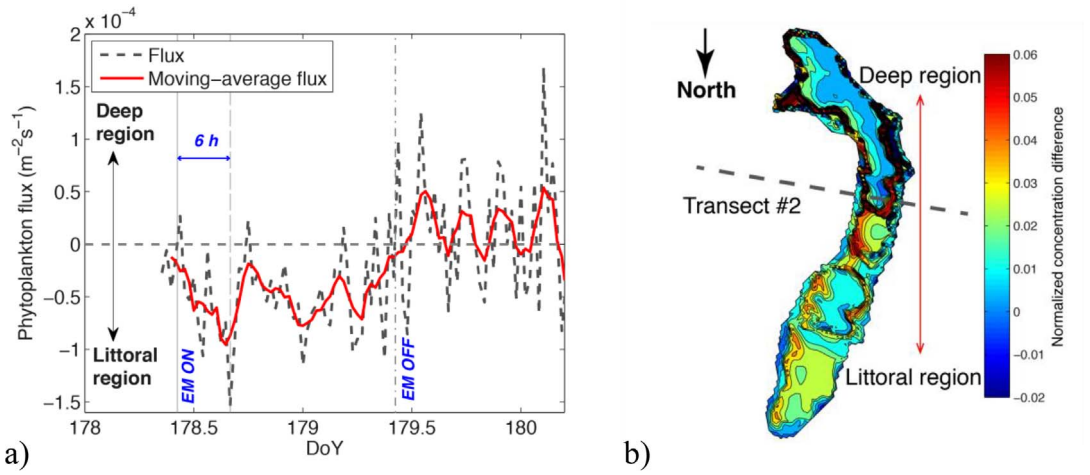

Fig. 5. Results from Case 2: a) mean horizontal fluxes of the phytoplankton concentration (normalized by the initial phytoplankton concentration) at Transect #2 (dashed black plot) and the time-moving-averaged (30 min) fluxes (red plot): positive values mean moving towards the deep region (FCR50); negative values mean moving towards the shallow region (FCR10). The solid vertical line indicates the beginning of bubble-plume mixing; the dashed vertical line indicates the time instant at 6 h after the mixing commenced; and the dash-dotted vertical line indicates the end of bubble-plume mixing. b) Contour of normalized phytoplankton concentration difference above the sediments before EM at 0 h and during EM at 6 h: the concentration is normalized by the initial phytoplankton concentration and calculated by the contour of 6 h minus that of 0 h. The flux of phytoplankton at 6 h is shown in a). (For interpretation of the references to colour in this figure legend, the reader is referred to the web version of this article.)

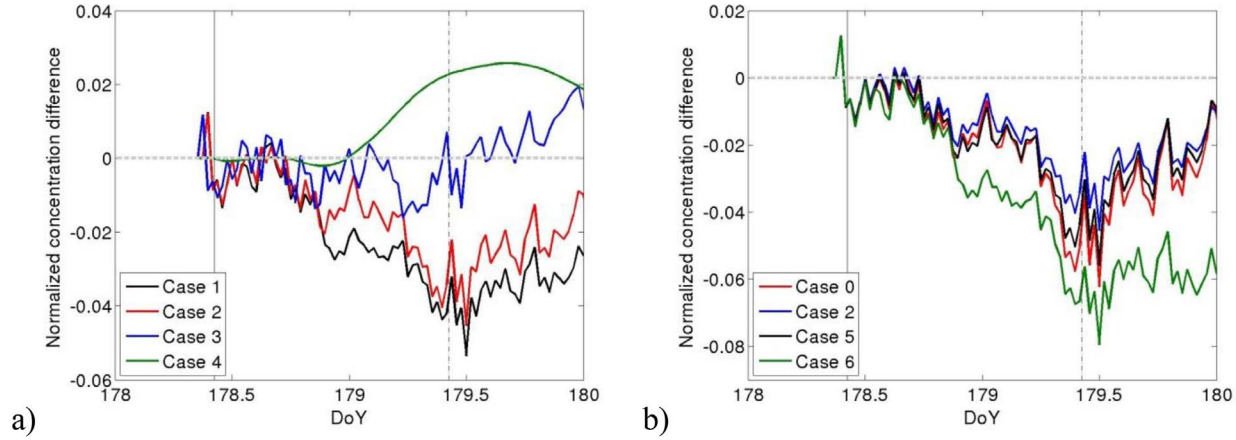

Fig. 6. Difference of phytoplankton concentration with and without induced mixing (normalized by the initial phytoplankton concentration) for cases with a) phytoplankton settling only (growth rates are set to zero); and b) phytoplankton settling and growth. A negative value means the mean concentration over the water body decreases due to induced mixing.

Table 3
Simulation cases of various growth parameters.

Cases	0	2	5	6
G	0.9	0.0	0.5	2.2

Table 4
Simulation cases of various bathymetries.

Cases	Maximum Depth (m)	Settling Rate (m/d)	Growth Rate (d^{-1})	Diffuser Depth (m)
0 (reference)	9.3	1.2	0.12	5.00
7	14.0	1.2	0.12	7.50
8	16.8	1.2	0.12	8.75
9	18.6	1.2	0.12	10.0
10	23.3	1.2	0.12	12.5
11	28.0	1.2	0.12	15.0
12	32.6	1.2	0.12	17.5

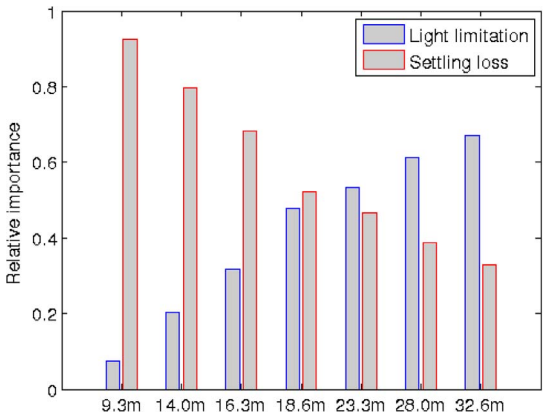

Fig. 7. Relative importance of the light limitation vs settling loss on phytoplankton cells in water bodies with various maximum depths.

Table 5
Simulation cases of various diffuser depths.

Cases	Maximum Depth (m)	Settling Rate (m/d)	Growth Rate (d^{-1})	Diffuser Depth (m)
0 (reference)	9.3	1.2	0.12	5.00
11	28.0	1.2	0.12	15.0
13	28.0	1.2	0.12	5.00
14	28.0	1.2	0.12	*

*Diffuser is located at 1 m above the sediments.

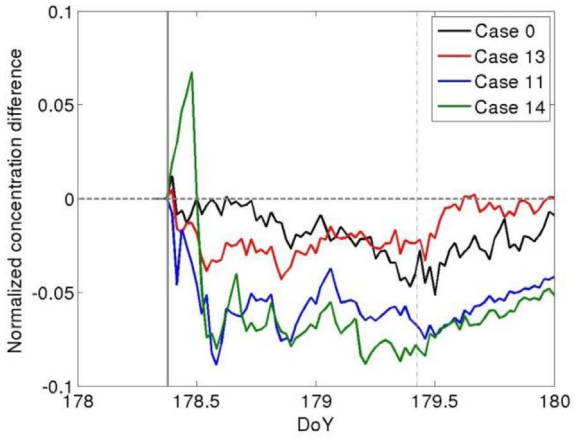

Fig. 8. Difference of phytoplankton concentration with and without induced mixing (normalized by the initial phytoplankton concentration) for the cases with the various depths of diffuser compared to the reference case. A negative value means the mean concentration over the water body decreases under the effect of induced mixing. The legend is ordered by ascending diffuser depths.

concentration of heavier taxa (e.g., diatoms) by keeping them suspended in the water column. The same outcomes are also reported in the literature (Huisman et al., 2004; Imteaz et al., 2009; Visser et al., 2016). The outcome of induced mixing tends to be more effective for phytoplankton cells with a higher growth rate (i.e., $G > 1$). The identified results may help explain the inconsistent results observed in previous studies of bubble-plume mixing systems (e.g., Nürnberg et al., 2003), in which it may be more likely for bubble-plume mixing to reduce fast-growing taxa rather than the relatively slow-growing cyanobacteria.

Light limitation is identified as a significant factor that constrains the phytoplankton concentration when the maximum water depth is > 20 m. Induced mixing could deepen the depth of phytoplankton cells so that their growth can be restrained by the reduced light availability in the aphotic zone (Visser et al., 2016). In deeper water bodies where the effect of light limitation is important, the reduction of phytoplankton concentration becomes more substantial with a higher mixing intensity and a greater mixing depth, which may be attained by lowering the diffuser depth while keeping the same DMPR. However, the potential of premature destratification may increase if the diffuser of mixing systems is placed in deeper water (e.g., Toffolon et al., 2013). This trade-off for phytoplankton management needs to be considered by lake and reservoir managers.

4. Recommendations

This combined field and numerical study demonstrates the importance of three-dimensional modelling of phytoplankton to predict their responses to bubble-plume mixing. For example, this study found that taxa with less dense cells (i.e., cyanobacteria) can be transported laterally to the upstream shallow region in reservoirs by the flows induced by bubble-plume mixing, resulting in substantial reduction of the cell concentration due to relatively shorter distance for settling on the sediments. The induced mixing may also enable the taxa with heavier cells (i.e., diatoms) to survive in the water body (Visser et al., 2016), which is a preferable outcome for water management. This management outcome is consistent with the cases reported in the literature (Huisman et al., 2004; Visser et al., 2016), even though the present mechanism responsible for the mixing and transport is different from that reported previously. Thus, taking into account vertical migration and settling rates of the cells is important (Visser et al., 1997; Carey et al., 2014), especially when using bubble-plume mixing to manage phytoplankton in shallow water bodies.

Reducing the growth rate of bloom-forming cyanobacteria is often a goal of water quality management. In this case, light limitation becomes a dominant driver for limiting phytoplankton growth in water bodies (Huisman et al., 2004) if the maximum water depth is deep (e.g., > 20 m). In contrast, induced mixing in shallower water bodies is likely to be less effective in reducing the light-dependent growth rate of cyanobacteria because those lakes and reservoirs do not have a sufficiently large aphotic zone.

Although placing the diffuser in deeper water with higher flow rates may lead to better performance in terms of reducing cyanobacteria, the potential of thermal destratification also increases. The trade-off between reducing harmful phytoplankton cells and preserving thermal stratification should be considered for reservoir management. For future bubble-plume mixing applications, these results suggest that mixing diffusers should be deployed in deep regions of water bodies so that more phytoplankton can be entrained by the mixing flows. The depth of the diffuser also needs to be chosen appropriately (e.g., half of the maximum depth as in FCR) to preserve thermal stratification.

The present study provides promising results for simulating phytoplankton dynamics in lakes and reservoirs using the coupled Si3D-AED model, with the goal of improving the design and operation of bubble-plume mixing systems. Future modelling and field studies should classify the phytoplankton taxa into specific species and include additional environmental variables (e.g., nutrients and carbon) using a whole-ecosystem approach, which will enable the prediction of 3-D phytoplankton dynamics over longer time scales. These next steps would greatly advance our understanding of how best to improve the management of phytoplankton community dynamics using diffuser mixer systems.

Acknowledgements

We thank J. Doubek, N. Ward, C. Harrell, and K. Krueger for their assistance with field data collection. We thank the staff at the Western Virginia Water Authority for support of this research, especially R. Benninger, J. Booth, C. Brewer, J. Morris, and G. Robertson. We also thank the Reservoir Group at Virginia Tech for their thoughtful comments regarding the project. P. Gantzer and M. Mobley provided critical help in the field with the SSS and EM systems. We acknowledge the open-source FABM and its documentation in the SourceForge and GitHub repositories. We acknowledge financial assistance from the School of Civil Engineering, The University of Sydney, the Department of Civil and Environmental Engineering at Virginia Tech, and U.S. National Science Foundation grants CNS-1737424 and EF-1702506. This research was also financially supported by the Fralin Life Sciences Institute and Global Change Center at Virginia Tech.

Appendix 1

See Appendix 1.

Appendix 1
Parameters in the phytoplankton module of AED. Other parameters (e.g., nutrients) were not included due to the focus on the physics in the study.

Parameters	Description	Value	Note
$P_{initial}$	Initial concentration of phytoplankton (mmol C/m^3)	–	Overridden by hydrodynamic model
P_0	Minimum concentration of phytoplankton (mmol C/m^3)	0.003	AED manual
w_p	Sedimentation rate (m/d)	–	Refer to case (Reynolds et al., 1987)
Y_{cc}	Carbon to chlorophyll ratio (mg C/mg chla)	40	AED manual
R_G	Phytoplankton growth rate (d^{-1})	–	Refer to case (Welschmeyer and Lorenzen, 1985)
I_{ST}	Saturating light intensity (microE/m^2/s)	150	AED manual
K_{ePHY}	Specific attenuation coefficient (mmol C/m^2)	0.005	AED manual

References

Bailey, M.C., Hamilton, D.P., 1997. Wind induced sediment resuspension: a lake-wide model. Ecol. Model. 99 (2), 217–228.

Bielczyńska, A., 2015. Bioindication on the basis of benthic diatoms: advantages and disadvantages of the Polish phytobenthos lake assessment method (IOJ – the Diatom Index for Lakes)/Bioindykacja na podstawie okrzemek bentosowych: Mocne i słabe strony polskiej metody oceny jezior na podstawie fitobentosu (IOJ – Indeks Okrzemkowy Jezior).

Brookes, J.D., Carey, C.C., 2011. Resilience to blooms. Science 334 (6052), 46–47.

Bruggeman, J., Bolding, K., 2014. A general framework for aquatic biogeochemical models. Environ. Modell. Software 61, 249–265.

Carey, C.C., Weathers, K.C., Ewing, H.A., Greer, M.L., Cottingham, K.L., 2014. Spatial and temporal variability in recruitment of the cyanobacterium Gloeotrichia echinulata in an oligotrophic lake. Freshwater Sci. 33 (2), 577–592.

Carey, C.C., Ewing, H.A., Cottingham, K.L., Weathers, K.C., Thomas, R.Q., Haney, J.F., 2012. Occurrence and toxicity of the cyanobacterium Gloeotrichia echinulata in low-nutrient lakes in the northeastern United States. Aquat. Ecol. 46 (4), 395–409.

Cerc, U.A., 1984. Shore Protection Manual. US Army Corps of Engineers, Washington.

Chen, S., Lei, C., Carey, C.C., Gantzer, P.A., Little, J.C., 2017. A coupled three-dimensional hydrodynamic model for predicting hypolimnetic oxygenation and epilimnetic mixing in a shallow eutrophic reservoir. Water Resour. Res. 53 (1).

Chiou, W., Faas, R., Kasprowicz, J., Li, H., Lomenick, T., OBrien, N., Pamukcu, S., Smart, P., Weaver, C., Yamamoto, T., 2012. Microstructure of Fine-grained Sediments: From Mud to Shale. Springer Science & Business Media.

Condie, S.A., 1999. Settling regimes for non-motile particles in stratified waters. Deep Sea Res. Part I 46 (4), 681–699.

Condie, S.A., Bormans, M., 1997. The influence of density stratification on particle settling, dispersion and population growth. J. Theor. Biol. 187 (1), 65–75.

Curran, K.J., Hill, P.S., Milligan, T.G., Mikkelsen, O.A., Law, B.A., Durrieu de Madron, X., Bourrin, F., 2007. Settling velocity, effective density, and mass composition of suspended sediment in a coastal bottom boundary layer, Gulf of Lions, France. Continental Shelf Res. 27 (10), 1408–1421.

Durham, W.M., Climent, E., Barry, M., De Lillo, F., Boffetta, G., Cencini, M., Stocker, R., 2013. Turbulence drives microscale patches of motile phytoplankton. Nat. Commun. 4, 2148.

Eppley, R.W., Holmes, R.W., Strickland, J.D.H., 1967. Sinking rates of marine phytoplankton measured with a fluorometer. J. Exp. Mar. Biol. Ecol. 1 (2), 191–208.

Gerling, A.B., Browne, R.G., Gantzer, P.A., Mobley, M.H., Little, J.C., Carey, C.C., 2014. First report of the successful operation of a side stream supersaturation hypolimnetic oxygenation system in a eutrophic, shallow reservoir. Water Res. 67, 129–143.

Heo, W.-M., Kim, B., 2004. The effect of artificial destratification on phytoplankton in a reservoir. Hydrobiologia 524 (1), 229–239.

Hipsey, M.R., Bruce, L.C., Hamilton, D.P., 2013. GLM general lake model, in Model overview and user information, The University of Western Australia, Perth, Australia.

Huisman, J., Matthijs, H.C.P., Visser, P.M., 2005. Harmful Cyanobacteria. Springer, Dordrecht.

Huisman, J., Sharples, J., Stroom, J.M., Visser, P.M., Kardinaal, W.E.A., Verspagen, J.M.H., Sommeijer, B., 2004. Changes in turbulent mixing shift competition for light between phytoplankton species. Ecology 85 (11), 2960–2970.

Imteaz, M.A., Asaeda, T., 2000. Artificial mixing of lake water by bubble plume and effects of bubbling operations on algal bloom. Water Res. 34 (6), 1919–1929.

Imteaz, M.A., Shanableh, A., Asaeda, T., 2009. Modelling multi-species algal bloom in a lake and inter-algal competitions. Water Sci. Technol. 60 (10), 2599–2611.

James, W.F., Barko, J.W., Butler, M.G., 2004. Shear stress and sediment resuspension in relation to submersed macrophyte biomass. Hydrobiologia 515 (1), 181–191.

Kamykowski, D., McCollum, S.A., 1986. The temperature acclimatized swimming speed of selected marine dinoflagellates. J. Plankton Res. 8 (2), 275–287.

Khelifa, A., Hill, P.S., 2006. Models for effective density and settling velocity of flocs. J. Hydraul. Res. 44 (3), 390–401.

Lehman, J.T., 2014. Understanding the role of induced mixing for management of nuisance algal blooms in an urbanized reservoir. Lake Reservoir Manage. 30 (1), 63–71.

Nürnberg, G.K., LaZerte, B.D., Olding, D.D., 2003. An artificially induced planktothrix rubescens surface bloom in a small kettle lake in southern ontario compared to blooms world-wide. Lake Reservoir Manage. 19 (4), 307–322.

Parker, J.A., Kenyon, R.V., Troxel, D.E., 1983. Comparison of interpolating methods for image resampling. IEEE Trans. Med. Imaging 2 (1), 31–39.

Reynolds, C.S., 2006. The Ecology of Phytoplankton. Cambridge University Press.

Reynolds, C.S., Oliver, R.L., Walsby, A.E., 1987. Cyanobacterial dominance: the role of buoyancy regulation in dynamic lake environments. N. Z. J. Mar. Freshwater Res. 21 (3), 379–390.

Rigosi, A., Fleenor, W., Rueda, F., 2010. State-of-the-art and recent progress in phytoplankton succession modelling. Environ. Rev. 18 (NA), 423–440.

Rueda, F.J., Schladow, S.G., 2003. Dynamics of large polymictic lake. II: Numerical simulations. J. Hydraul. Eng. 129 (2), 92–101.

Rueda, F.J., Sanmiguel-Rojas, E., Hodges, B.R., 2007. Baroclinic stability for a family of two-level, semi-implicit numerical methods for the 3D shallow water equations. Int. J. Numer. Meth. Fluids 54 (3), 237–268.

Singleton, V.L., Gantzer, P., Little, J.C., 2007. Linear bubble plume model for hypolimnetic oxygenation: full-scale validation and sensitivity analysis. Water Resour. Res. 43 (2).

Singleton, V.L., Rueda, F.J., Little, J.C., 2010. A coupled bubble plume-reservoir model for hypolimnetic oxygenation. Water Resour. Res. 46 (12).

Smith, P.E., 2006. A semi-Implicit, three-dimensional model for estuarine circulation.

Toffolon, M., Ragazzi, M., Righetti, M., Teodoru, C.R., Tubino, M., Defrancesco, C., Pozzi, S., 2013. Effects of artificial hypolimnetic oxygenation in a shallow lake. Part 1: Phenomenological description and management. J. Environ. Manage. 114, 520–529.

Visser, P., Ibelings, B., Bormans, M., Huisman, J., 2016. Artificial mixing to control cyanobacterial blooms: a review. Aquat. Ecol. 1–19.

Visser, P.M., Passarge, J., Mur, L.R., 1997. Modelling vertical migration of the cyanobacterium microcystis. Hydrobiologia 349 (1), 99–109.

Welschmeyer, N.A., Lorenzen, C.J., 1985. Chlorophyll budgets: zooplankton grazing and phytoplankton growth in a temperate fjord and the Central Pacific Gyres1. Limnol. Oceanography 30 (1), 1–21.

Wüest, A., Brooks, N.H., Imboden, D.M., 1992. Bubble plume modeling for lake restoration. Water Resour. Res. 28 (12), 3235–3250.